Acta Crystallographica Section D
Biological Crystallography
ISSN 0907-4449

Structure of the Calx-β domain of the integrin β4 subunit: insights into function and cation-independent stability

Noelia Alonso-García,[a] Alvaro Inglés-Prieto,[a]‡ Arnoud Sonnenberg[b] and Jose M. de Pereda[a]*

[a]Instituto de Biología Molecular y Celular del Cáncer, Consejo Superior de Investigaciones Científicas–Universidad de Salamanca, Campus Unamuno, 37007 Salamanca, Spain, and [b]Netherlands Cancer Institute, Plesmanlaan 121, 1066 CX Amsterdam, The Netherlands

‡ Present address: Departamento de Química-Física, Facultad de Ciencias, Campus Fuentenueva, 18071 Granada, Spain.

Correspondence e-mail: pereda@usal.es

Received 9 January 2009
Accepted 18 May 2009

PDB References: Calx-β domain of integrin β4, 3fq4, r3fq4sf; 3h6a, r3h6asf; 3fso, r3fsosf.

The integrin $\alpha6\beta4$ is a receptor for laminins and provides stable adhesion of epithelial cells to the basement membranes. In addition, $\alpha6\beta4$ is important for keratinocyte migration during wound healing and favours the invasion of carcinomas into surrounding tissue. The cytoplasmic domain of the $\beta4$ subunit is responsible for most of the intracellular interactions of the integrin; it contains four fibronectin type III domains and a Calx-β motif. The crystal structure of the Calx-β domain of $\beta4$ was determined to 1.48 Å resolution. The structure does not contain cations and biophysical data support the supposition that the Calx-β domain of $\beta4$ does not bind calcium. Comparison of the Calx-β domain of $\beta4$ with the calcium-binding domains of Na^+/Ca^{2+}-exchanger 1 reveals that in $\beta4$ Arg1003 occupies a position equivalent to that of the calcium ions in the Na^+/Ca^{2+}-exchanger. By combining mutagenesis and thermally induced unfolding, it is shown that Arg1003 contributes to the stability of the Calx-β domain. The structure of the Calx-β domain is discussed in the context of the function and intracellular interactions of the integrin $\beta4$ subunit and a putative functional site is proposed.

1. Introduction

Integrins are a family of cell-surface adhesion receptors that transmit bidirectional signals between the cytoplasm and the extracellular milieu (Hynes, 2002; van der Flier & Sonnenberg, 2001). Integrins are heterodimeric receptors composed of one α subunit and one β subunit; the subunits are noncovalently associated. The α and β subunits are type I transmembrane glycoproteins consisting of a large multi-domain extracellular region involved in the recognition of ligands, a single transmembrane α-helix and typically short cytoplasmic moieties that contain the C-terminus and are responsible for interaction with intracellular activators and effectors (Arnaout *et al.*, 2007; Wegener & Campbell, 2008).

In mammals, there are 18 α and eight β integrin subunits that combine to form 24 $\alpha\beta$ receptors. The $\beta4$ subunit only exists in combination with $\alpha6$ in the $\alpha6\beta4$ integrin, which is a receptor for laminins (Wilhelmsen *et al.*, 2006). In complex and stratified epithelia $\alpha6\beta4$ is located at the basal layer of cells, where it is a component of junctional complexes named hemidesmosomes that mediate stable adhesion to the underlying basement membrane (Litjens *et al.*, 2006; Nievers *et al.*, 1999). In addition to the role of $\alpha6\beta4$ in stable adhesion, $\alpha6\beta4$ favours keratinocyte migration during wound healing and $\alpha6\beta4$ signalling promotes carcinoma invasion (Giancotti, 2007; Lipscomb & Mercurio, 2005; Wilhelmsen *et al.*, 2006).

The $\beta4$ subunit has a unique cytoplasmic domain which is much larger (~1000 amino acids) than those of other β sub-

units and shares no sequence similarity with them. The function of the $\alpha6\beta4$ integrin relies on the cytoplasmic domain of $\beta4$. This domain acts as an adaptor platform that engages in protein–protein interactions both for the assembly of hemidesmosomes and for $\alpha6\beta4$ signalling. The $\beta4$ cytoplasmic moiety has a mosaic domain organization and is composed of sequentially arranged domains (Fig. 1*a*). It contains four fibronectin type III (FnIII) domains arranged in two pairs of tandem repeats separated by a region termed the connecting segment. A 90-residue-long C-terminal tail extends downstream of the fourth FnIII domain. Upstream of the first FnIII domain there is a region that is homologous to the Calx-β sequence motif (Schwarz & Benzer, 1997).

The Calx-β motif was first identified in the cytoplasmic region of Na^+/Ca^{2+}-exchangers (NCX; Schwarz & Benzer, 1997), a family of plasma-membrane proteins that contribute to Ca^{2+} homeostasis by expelling Ca^{2+} from the cytoplasm (Lytton, 2007). NCXs have a large intracellular domain that contains two copies in tandem of the Calx-β motif, which correspond to two Ca^{2+}-binding domains (CBD1 and CBD2; Hilge *et al.*, 2006). In addition to NCXs and $\beta4$, Calx-β repeats are also present in the ectodomain of the very large G protein-coupled receptor 1 (Nikkila *et al.*, 2000), the MAFp3 aggregation factor of the marine sponge *Microciona prolifera* (Fernandez-Busquets *et al.*, 1996), extracellular matrix protein 3 of sea urchin (Hodor *et al.*, 2000), members of the 12-CSPG family of extracellular matrix proteins (Kiyozumi *et al.*, 2007), the membrane-bound β-glucosidase BglM1 from *Physarum polycephalum* (Hayase *et al.*, 2008) and proteins from the cyanobacterium *Synechocystis* sp. PCC6803 (Schwarz & Benzer, 1997). The structures of CBD1 and CBD2 of Na^+/Ca^{2+}-exchanger 1 (NCX1) have recently been determined by NMR and X-ray crystallography (Besserer *et al.*, 2007; Hilge *et al.*, 2006; Nicoll *et al.*, 2006). The Calx-β domain adopts a classical immunoglobulin fold that consists of a β-sandwich built up of two β-sheets. The CBDs bind two or four Ca^{2+} ions

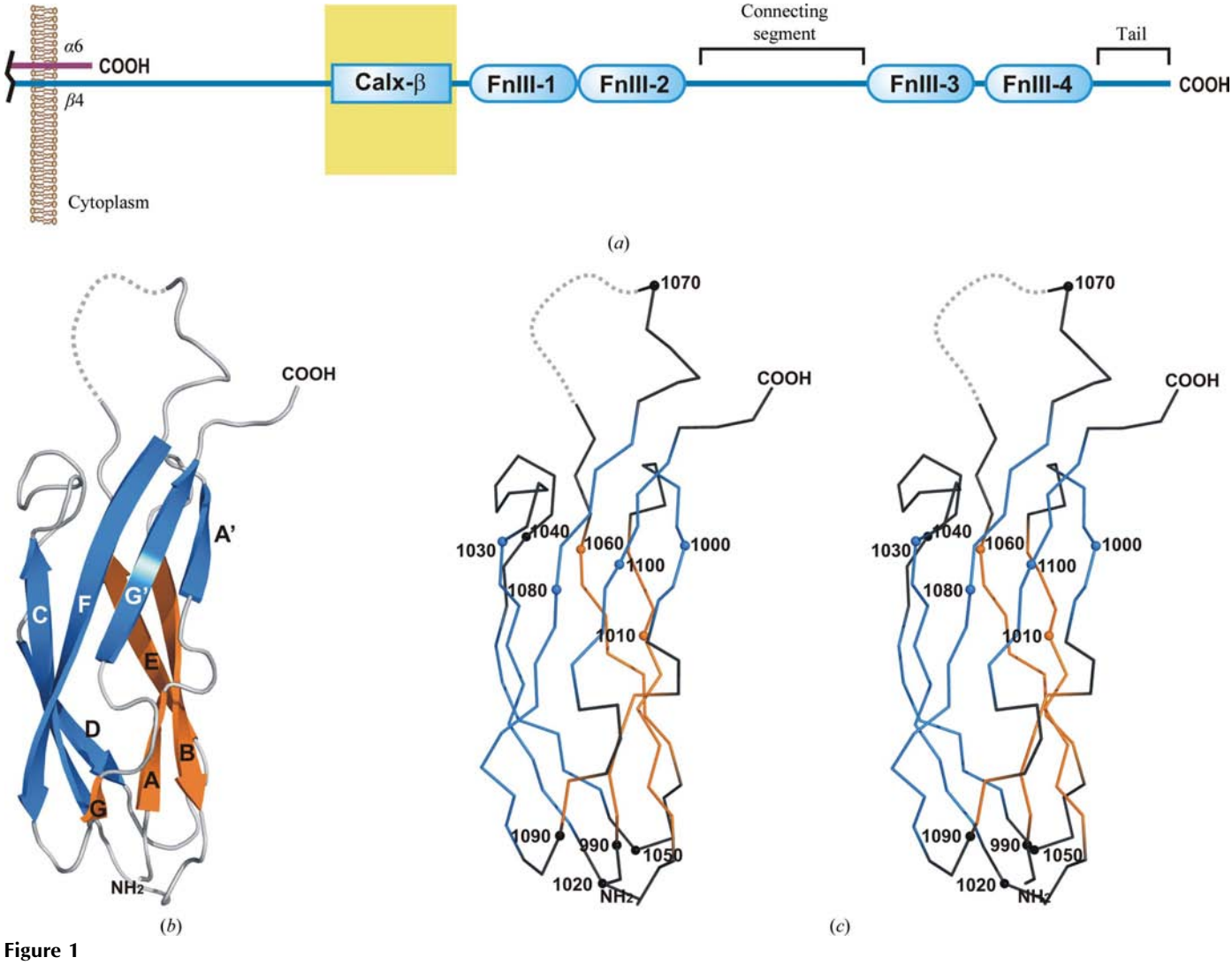

Figure 1
Structure of the Calx-β domain of $\beta4$. (*a*) Domain organization of the cytoplasmic moiety of the $\alpha6\beta4$ integrin. The Calx-β domain whose structure is presented here is highlighted by a yellow box. (*b*) Ribbon representation of the structure of the Calx-β domain of $\beta4$. The β-strands that form each of the two β-sheets of the domain are shown in the same colour. Part of the *EF* loop was disordered in the structure and is represented by a dashed line. (*c*) Stereo C^{α}-trace representation in the same orientation and using the same colour code as in (*b*). The position of every tenth residue is labelled.

at sites that are located adjacent to each other at one end of the β-sandwich, in which the Ca^{2+} ions are coordinated by acidic residues. Based on sequence comparison, the Ca^{2+}-binding site is not fully conserved in the Calx-β domain of β4, suggesting that it does not bind Ca^{2+} or other divalent cations (Hilge *et al.*, 2006). In contrast to the major breakthroughs in structural determination of the Ca^{2+}-binding Calx-β domains of NCX1, no structures of a non-Ca^{2+}-binding Calx-β domain have been described to date.

The role of the Calx-β domain of β4 in the function of $\alpha6\beta4$ integrin is not known. The function of $\alpha6\beta4$ integrin has not been reported to be directly regulated by Ca^{2+} to date, suggesting that in β4 the Calx-β domain does not act as a Ca^{2+} sensor. A region of β4 that extends between the transmembrane region and the first FnIII, which includes the Calx-β domain, mediates the association of $\alpha6\beta4$ with the tyrosine kinase Fyn in response to epidermal growth factor (EGF) stimulation (Mariotti *et al.*, 2001), suggesting that the Calx-β domain of β4 may have a role in protein–protein interactions.

Knowledge of the structure of $\alpha6\beta4$ is limited to the crystal structures of the first pair of tandem FnIII domains of β4 (de Pereda *et al.*, 1999, 2009), a region that is essential for interaction with the cytoskeletal protein plectin and for the formation of hemidesmosomes (Niessen *et al.*, 1997). The structural determinants for the interaction between the first pair of FnIII domains of β4 and the actin-binding domain of plectin at the hemidesmosomes have recently been defined (de Pereda *et al.*, 2009). In order to expand our knowledge of the structure of the $\alpha6\beta4$ integrin and in particular to better understand the structure and possible function of the Calx-β domain of β4, we have determined the crystal structure of this domain and have analyzed whether it interacts with Ca^{2+}.

2. Materials and methods

2.1. Sample preparation

The cDNA sequence coding for the Calx-β domain (residues 989–1107) of human integrin β4 (Uniprot accession No. P16144) was amplified by the polymerase chain reaction (PCR) using IMAGE clone 3640058 as a template. The forward primer (5′-TGAGAATTCCATATGAGAGACGTG-GTGTCCTTTGAGC-3′) contains an *Eco*RI site and an *Nde*I site, while the reverse primer (5′-GCCGAATTCGGATCCC-TATTCATCTGGGTCCCTGATG-3′) contains a stop codon, a *Bam*HI site and an *Eco*RI site. The amplified DNA was digested with *Eco*RI and inserted into the pBluescript SK(−) vector (Stratagene). Subsequently, the cDNA fragment produced by digestion with *Nde*I and *Bam*HI was cloned into a derivative of the pET15b vector (Novagen) which codes for an octa-His tag and a site recognized by the tobacco etch virus (TEV) protease at the N-terminus of the fusion protein (amino-acid sequence MGSSHHHHHHHHSSGENLYFQG-SHM). The Calx-β domain was expressed in *Escherichia coli* strain BL21 (DE3) carrying the recombinant plasmid. Bacteria were grown in Terrific Broth medium (Sambrook *et al.*, 1989) supplemented with 100 mg l^{-1} ampicillin. Expression of the recombinant protein was induced by incubation with 0.2 m*M* IPTG for 3 h at 310 K. Cells were harvested, resuspended in 20 m*M* Tris–HCl pH 7.9, 500 m*M* NaCl, 5 m*M* imidazole and lysed by sonication. After centrifugation at 40 000*g* for 30 min at 277 K, the target protein was present in the insoluble fraction and was solubilized in 20 m*M* Tris–HCl pH 7.9, 500 m*M* NaCl, 5 m*M* imidazole, 6 *M* urea. The Calx-β domain was purified by nickel-chelating affinity chromatography and was eluted with 20 m*M* Tris–HCl pH 7.9, 500 m*M* NaCl, 400 m*M* imidazole, 6 *M* urea. The Calx-β domain was refolded by 20-fold dilution in 20 m*M* Tris–HCl pH 7.5, 150 m*M* NaCl, 1 m*M* EDTA, which resulted in a residual urea concentration of 0.3 *M*. Insoluble material was removed by centrifugation (40 000*g*, 30 min, 277 K) and the soluble protein was concentrated to $\sim$2 mg ml^{-1} by ultrafiltration using YM3 membranes (Amicon). The yield of the refolding step was $\sim$39%. The His tag was cleaved by digestion with TEV and was removed by a second nickel-chelating affinity chromatography step under nondenaturing conditions. Finally, the sample was extensively dialyzed against 10 m*M* Tris–HCl pH 7.5, 50 m*M* NaCl and was concentrated to the desired concentration by ultrafiltration.

Two single point mutants, R1003A and R1003E, of the Calx-β domain in the pET15b-derivative vector were created by site-directed mutagenesis using the QuikChange method (Stratagene). The substitution R1003A was introduced using the primers 5′-GAGTTCTCGGTCAGCGCCGGG-TCGGTCAGCGCCGGGGACCAGGTGGCC-3′ and 5′-GGCCACCTGGTCCCCGGCGCTGACCGAGAACTC-3′, while the R1003E substitution was created using the primers 5′-GAGTTCTCGGTCAGCGAGGGGGACCAGGTGGCC-3′ and 5′-GGCCACCTGGTCCCCCTCGCTGACCGAGAA-CTC-3′. The correctness of the sequences was verified by DNA sequencing. The mutant proteins were purified and refolded as for the wild-type protein.

The molecular masses of the wild-type, R1003A and R1003E proteins were determined by MALDI–TOF to be 13 955, 13 863 and 13 920 Da, respectively. The experimental values were in agreement with the theoretical masses (wild type, 13 947 Da; R1003A, 13 862 Da; R1003E, 13 920 Da) within experimental error.

2.2. Crystallization and data collection

Initial crystallization screening was performed by the oil-microbatch method using 384 ShallowWell plates (Nunc) and a commercial collection of 432 crystallization solutions which were assayed at 277 and 295 K. After optimization of the initial conditions, crystals were grown at 295 K using the vapour-diffusion method by mixing 3.5 µl Calx-β domain at 24 mg ml^{-1} in 10 m*M* Tris–HCl pH 7.5, 50 m*M* NaCl with 4.5 µl 50 m*M* Tris–HCl pH 8.3, 26% PEG 1500. Prior to data collection, crystals were transferred to 50 m*M* Tris–HCl pH 8.3, 26% PEG 1500, 15% glycerol and were flash-frozen by direct immersion in liquid nitrogen. Crystals were also grown in the presence of Ca^{2+} using 50 m*M* Tris–HCl pH 7.9, 2 m*M* $CaCl_2$, 26% PEG 1500 as the crystallization solution. Crystals

Table 1
Summary of crystallographic analysis.

Values in parentheses are for the outer resolution shell.

	Native	2 m*M* Ca^{2+} cocrystal	10 m*M* Ca^{2+} soak
Data collection			
Space group	$P2_12_12_1$	$P2_12_12_1$	$P2_12_12_1$
Unit-cell parameters			
a (Å)	50.3	50.3	50.3
b (Å)	51.7	51.7	51.7
c (Å)	87.5	87.4	87.4
Wavelength (Å)	1.5418	1.5418	1.5418
Resolution (Å)	1.48 (1.54–1.48)	1.61 (1.69–1.61)	1.40 (1.50–1.40)
Unique reflections	38089 (3644)	30229 (4045)	44715 (7607)
Redundancy	13.4 (11.3)	9.2 (8.3)	12.7 (10.7)
Completeness (%)	98.3 (85.4)	98.1 (88.1)	98.1 (91.1)
R_{meas}† (%)	5.3 (31.2)	9.3 (33.8)	8.3 (24.5)
$\langle I/\sigma(I)\rangle$	29.5 (8.6)	17.1 (6.6)	20.5 (9.9)
Refinement statistics			
Resolution range (Å)	26–1.48 (1.52–1.48)	20–1.61 (1.66–1.61)	22–1.40 (1.44–1.40)
Unique reflections (work/free)	36177/1911	28711/1515	42471/2229
R_{work}/R_{free} (%)	15.5 (20.4)/18.9 (24.8)	17.2 (21.7)/21.2 (26.1)	18.2 (22.3)/21.2 (23.9)
No. of atoms			
Protein‡	3783 [1903]	3742 [1878]	3803 [1913]
Water	334	296	308
Average *B* value (Å^2)			
Wilson plot	14.8	11.4	9.9
Protein§	19.5/20.7	17.4/18.6	18.6/18.8
Water	29.0	25.8	26.5
R.m.s. deviations			
Bond lengths (Å)	0.008	0.010	0.007
Bond angles (°)	0.960	1.273	0.909
B factors, main chain (Å^2)	1.67	2.14	1.54
B factors, side chain (Å^2)	4.47	4.49	4.01
Ramachandran plot regions¶			
Favoured	215 [98.6%]	211 [97.7%]	214 [98.6%]
Additionally allowed	3 [1.4%]	5 [2.3%]	3 [1.4%]
Disallowed	0	0	0
PDB code	3fq4	3h6a	3fso

† The multiplicity-independent *R* factor, $R_{meas} = \{\sum_{hkl}[n_{hkl}/(n_{hkl}-1)]^{1/2}\sum_i |I_i(hkl) - \langle I(hkl)\rangle|\}/\sum_{hkl}\sum_i I_i(hkl)$, where $I_i(hkl)$ is the *i*th measurement and $\langle I(hkl)\rangle$ is the mean of all measurements of $I(hkl)$ (Diederichs & Karplus, 1997) ‡ The number of atoms excluding H atoms is given in square brackets. § Values are given for each protein chain. ¶ Calculated with *MOLPROBITY* (Lovell *et al.*, 2003).

were transferred to 50 m*M* Tris–HCl pH 7.9, 2 m*M* $CaCl_2$, 27% PEG 1500, 15% glycerol and were flash-frozen in liquid nitrogen. Finally, crystals grown in the absence of Ca^{2+} were soaked for 1 h in 50 m*M* Tris–HCl pH 8.3, 10 m*M* $CaCl_2$, 25% PEG 1500 and were transferred into cryoprotectant solutions containing 10 m*M* $CaCl_2$ before freezing.

Diffraction images (1° oscillation) of native crystals and crystals soaked in 10 m*M* Ca^{2+} were collected at 100 K using a rotating-anode X-ray generator (MicrostarH, Bruker AXS) and a MAR 345dtb image-plate detector (MAR Research GmbH). Images of the crystal grown with 2 m*M* Ca^{2+} were collected at 110 K using a rotating-anode X-ray generator (FR591, Bruker AXS) and a MAR 345 detector (MAR Research GmbH). The high-resolution limit of the data was conditioned by the geometry of the diffractometers used to collect the data. All data were indexed with *XDS* and were scaled and reduced with *XSCALE* (Kabsch, 1993).

2.3. Structure solution and refinement

The crystals belonged to space group $P2_12_12_1$, with unit-cell parameters $a = 50.3$, $b = 51.7$, $c = 87.5$ Å, and contained two Calx-β molecules in the asymmetric unit (40% solvent content). The structure was solved and refined using a highly redundant data set that extended to a resolution of 1.48 Å (Table 1). The structure was phased by molecular replacement using the program *Phaser* (McCoy *et al.*, 2005). The search model was constructed by homology modelling based on the crystal structure of the first CBD of NCX1 (PDB code 2dpk; Nicoll *et al.*, 2006) and a profile-based sequence alignment obtained with the *FFAS*03 server (Jaroszewski *et al.*, 2005). The *SCWRL* server (Canutescu *et al.*, 2003) was used to create a mixed model that retained the side-chain rotamers of the residues conserved in β4, while nonconserved residues were mutated to Ser, with the exceptions of Ala and Gly residues in β4, which were trimmed to the C^{β} and C^{α} atoms, respectively. A search for two copies of the model with *Phaser* yielded a solution (log-likelihood gain = 114) in space group $P2_12_12_1$ which was significantly higher than any of the solutions that were obtained using the other possible primitive orthorhombic space groups. Refinement was performed with the program *phenix.refine* (Afonine *et al.*, 2005) against the structure-factor amplitudes of data to 1.48 Å resolution. Initially, the search models that were located in the molecular replacement were refined using simulated-annealing methods. The resulting likelihood-weighted maps ($2mF_{obs} - DF_{calc}$ and $mF_{obs} - DF_{calc}$) clearly revealed details of regions of the structure that were not included in the initial model (*e.g.* side chains) and allowed the unequivocal construction of most of the regions that were not present in the molecular-replacement model. Subsequently, bulk-solvent correction, positional and individual *B*-factor restrained refinement was alternated with manual model building using the program *Coot* (Emsley & Cowtan, 2004). The two molecules in the asymmetric unit were refined independently. The weight terms of the geometry and *B*-factor restraints were optimized during all refinement cycles. Six TLS groups (three in each molecule), which were identified using the *TLS Motion Determination* server (Painter & Merritt, 2006), were refined. Solvent molecules were built at peaks of over 4.5σ in $mF_{obs} - DF_{calc}$ maps if they had a level of at least 1.1σ in $2mF_{obs} - DF_{calc}$ maps and a reasonable hydrogen-bonding environment. During the final stages of refinement, H atoms were added and they were refined using a riding model. Four residues in molecule *A* (E995, R1009, R1027 and S1097) and seven residues in molecule *B* (S1002, E1043, E1045, Q1049, E1063, N1085 and S1097) were

modelled in two alternative conformations, the occupancies of which were refined. Refinement converged at R_{work} and R_{free} values of 15.5% and 18.9%, respectively (Table 1). The refined model had a superb geometry as determined using the *MOLPROBITY* validation server (Davis *et al.*, 2007). 98.6% of the main-chain torsion angles occupied favoured regions of the Ramachandran plot (Lovell *et al.*, 2003). Only Q1006 in both molecules and N1036 in molecule *A* lay in additionally allowed regions of the map, while no residues were in disallowed regions. The electron density of Q1006 is well defined in both molecules and confirms the unusual conformation of this residue (molecule *A*, $\varphi = 75^\circ$, $\psi = -16^\circ$; molecule *B*, $\varphi = 73^\circ$, $\psi = -41^\circ$; Supplementary Fig. 1[1]). In the structures of the CBD1 (PDB code 2dpk) and CBD2 (PDB code 2qvm) of NCX1, the residues equivalent to Q1006 are G388 ($\varphi = 82^\circ$, $\psi = -71^\circ$) and G519 ($\varphi = 86^\circ$, $\psi = -74^\circ$), respectively, which occupy regions of the Ramachandran plot that are disallowed for nonglycine residues. The final model contains residues 989–1064 and 1074–1105 of Calx-β molecule *A*, residues 989–1064 and 1069–1107 of molecule *B* and 334 solvent molecules. An additional Met coded by the vector was observed at the N-terminus of each of the two β4 molecules.

The crystals grown in the presence of 2 m*M* $CaCl_2$ were isomorphic with the native crystals (Table 1). The native structure (excluding the solvent molecules) was used as a starting model for the refinement, which was performed with the program *phenix.refine* (Afonine *et al.*, 2005) using the same subset of reflections for the calculation of the R_{free} as were used for the native structure. Initially, simulated annealing was used. Subsequently, refinement was performed as for the native structure except that six TLS groups were refined in each molecule. The final R_{work} and R_{free} values were 17.2% and 21.2%, respectively. The model contains residues 989–1064 and 1074–1105 of molecule *A*, residues 989–1064 and 1070–1107 of molecule *B* and 296 solvent molecules. The refined structure is almost identical to the native structure: the root-mean-square difference (r.m.s.d.) in the position of all C^α atoms between the native and Ca^{2+}-cocrystallized structures is 0.08 Å.

The crystals soaked in the presence of 10 m*M* $CaCl_2$ were also isomorphic with the native crystals (Table 1). The structure was refined in the same way as that of Calx-β crystallized in the presence of Ca^{2+}, with the exception of the refinement of 17 TLS groups in each molecule. The R_{free} was calculated using the same set of tagged reflections (5% of the data) as were used for the native crystals; the set was extended for the data between 1.48 and 1.40 Å that were not present in the native data set. Refinement converged at R_{work} and R_{free} values of 18.2% and 21.2%, respectively (Table 1). The r.m.s.d. in the position of all C^α atoms between the native and Ca^{2+}-soaked structures is 0.08 Å.

[1] Supplementary material has been deposited in the IUCr electronic archive (Reference: KW5011). Services for accessing this material are described at the back of the journal.

2.4. Structure analysis

Pairwise superposition of structures was performed with the program *DaliLite* (Holm & Park, 2000), which automatically identifies equivalent C^α atoms. Alternatively, the program *LSQKAB* (Kabsch, 1976) was used for pairwise superimposition and calculation of the r.m.s.d. using a common set of 100 equivalent C^α atoms consisting of Calx-β residues 990–1016, 1020–1035, 1037–1064, 1076–1088 and 1089–1104. Simultaneous superimposition of multiple structures was performed with the program *THESEUS* (Theobald & Wuttke, 2006), which uses a maximum-likelihood method. The protein interfaces, surfaces and assemblies service (*PISA*) at the European Bioinformatics Institute (Krissinel & Henrick, 2007) was used to analyze the crystal-packing interfaces. Molecular figures were prepared using the program *PyMOL* (DeLano, 2002).

2.5. Fluorescence-based thermal stability assay

Protein thermal unfolding was monitored using the thermofluor method (Pantoliano *et al.*, 2001), in which changes in the fluorescence of the environmentally sensitive probe Sypro Orange (Invitrogen) were measured as a function of the temperature. Assay samples (25 µl) consisted of 0.25 mg ml^{-1} protein and Sypro Orange (final concentration 10×; arbitrary concentration units defined by the manufacturer) in 50 m*M* HEPES pH 7.5, 150 m*M* NaCl buffer, which was supplemented with either 5 m*M* EGTA or 10 m*M* $CaCl_2$ when required. Experiments were performed using an IQ5 real-time PCR instrument (Bio-Rad) over a temperature range from 293 to 358 K with a heating rate of 1 K min^{-1}. Fluorescence measurements were collected every 0.5 K using a 480 nm (20 nm bandwidth) excitation filter and a 530 nm (30 nm bandwidth) emission filter. In order to accurately locate the inflection point of the melting transition (T_m), the first derivative of the fluorescence (arbitrary units) *versus* the temperature (dF/dT) was calculated.

2.6. Calcium-binding analysis by equilibrium dialysis

Samples (2 or 3 ml) of the Calx-β domain of β4 at ~200 µ*M* were extensively dialysed (five changes of 400 ml) at room temperature against solutions consisting of 20 m*M* Tris–HCl pH 7.5, 150 m*M* NaCl and various concentrations of $CaCl_2$. After dialysis, the protein concentration was determined spectrophotometrically using a value for the extinction coefficient at 280 nm of 8480 M^{-1} cm^{-1} calculated from the amino-acid composition of the Calx-β domain (Pace *et al.*, 1995). The concentration of Ca^{2+} in the dialysis buffers and in the protein samples was determined at the Applied Chemical Analysis Laboratory of the University of Salamanca using inductively coupled plasma optical emission spectrometry (ICP-OES). The concentration of Ca^{2+} bound to the Calx-β domain was determined by subtracting the concentration of Ca^{2+} in the buffer (free Ca^{2+}) from the concentration in the protein sample (free plus bound Ca^{2+}). The number of Ca^{2+} ions bound per Calx-β domain was calculated as the ratio between the bound Ca^{2+} and protein concentrations.

3. Results

3.1. Overall structure of the Calx-β domain of β4

The boundaries of the Calx-β motif of β4 have recently been redefined based on the NMR structures of CBD1 and CBD2 of NCX1 (Hilge *et al.*, 2006). The Calx-β domain of β4 (residues 989–1107) was expressed in *E. coli*, purified under denaturing conditions and refolded by rapid dilution. The sample produced by this method was suitable for crystallographic analysis.

The structure of Calx-β was phased by molecular replacement and was refined against data to 1.48 Å resolution (Table 1). The asymmetric unit of the crystals contained two β4 molecules related by a noncrystallographic dyad. The Calx-β domain is monomeric in solution, as determined by size-exclusion chromatography (data not shown). Thus, no

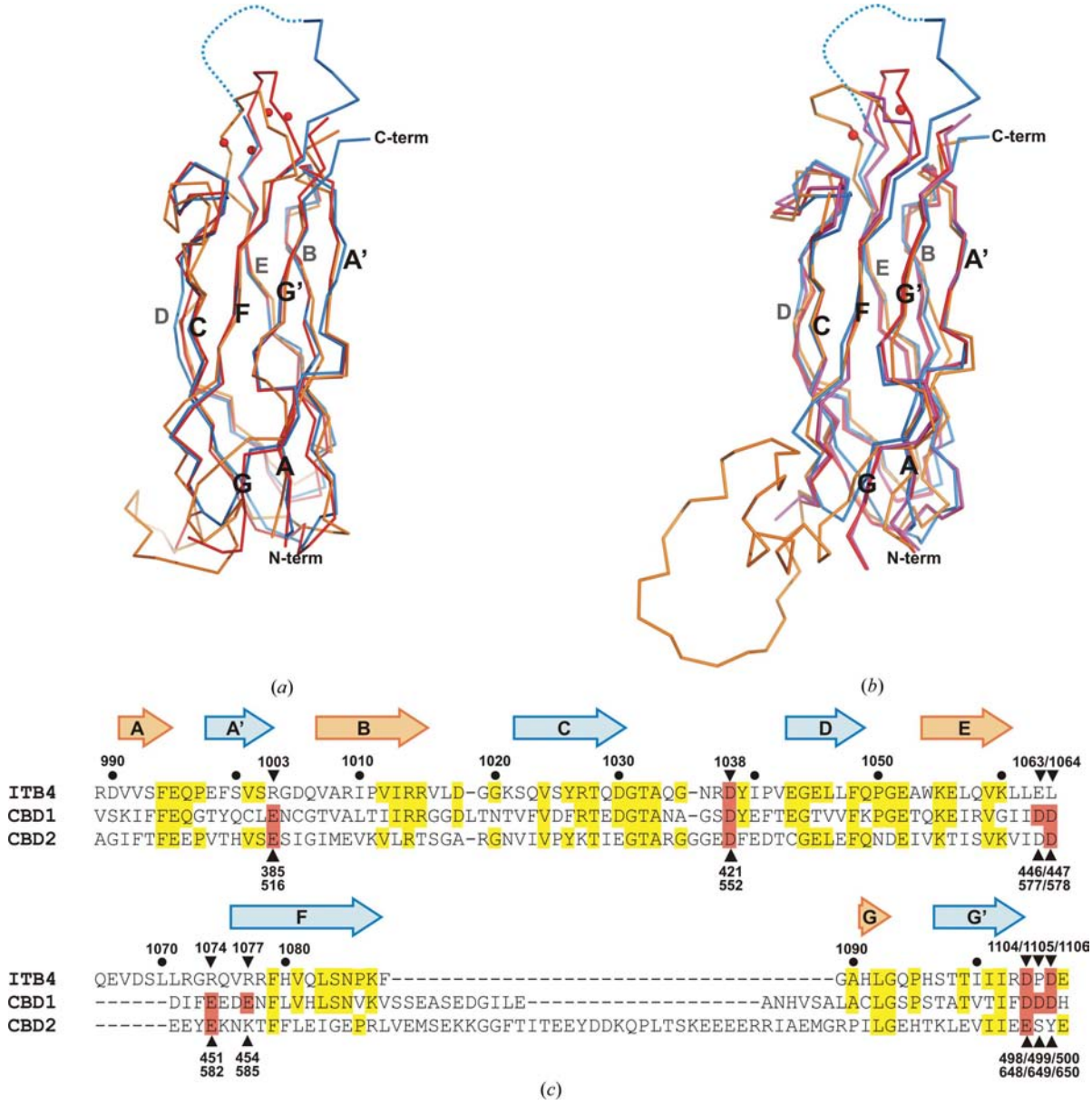

Figure 2
Comparison of the Calx-β domain of β4 with the Ca^{2+}-binding domains of Na^{+}/Ca^{2+}-exchanger 1. (*a*) C^{α}-trace superposition of the Calx-β domain of β4 (blue) and the NMR (orange; PDB code 2fws) and crystallographic (red; PDB code 2dpk) structures of CBD1 of NCX1. (*b*) C^{α}-trace superposition of the Calx-β domain of β4 (blue) and the NMR (orange; PDB code 2fwu) and crystallographic structures of CBD2 of NCX1 in the presence of Ca^{2+} (red; PDB code 2qvm) and in the absence of Ca^{2+} (magenta; PDB code 2qvk). The Ca^{2+} ions present in the CBD1 and CBD2 crystal structures are shown as red spheres. All the structures in (*a*) and (*b*) were superimposed simultaneously using a maximum-likelihood method. The orientation and the labelling of the β-strands are the same as in Fig. 1. (*c*) Structure-based sequence alignment of the β4 Calx-β domain (ITB4) and the CBD1 and CBD2 domains of NCX1. Secondary-structure elements in the β4 structure are indicated above the sequences and are coloured as in Fig. 1. Residues involved in the coordination of Ca^{2+} ions in the crystal structures of CBD1 and CBD2 are highlighted by red boxes and their numbers are shown below the sequences; the numbers of the equivalent residues in β4 are shown above the sequences. Residues conserved between β4 and CBD1 or CBD2 are highlighted by yellow boxes.

Table 2
Analysis of crystal contacts.

Molecule 1†	Molecule 2†	Interface area‡ (Å^2)	No. of hydrogen bonds	No. of salt bridges	Complexation significance score§
A	*B*	484	2	0	0
A	*B* ($x - 1/2, -y + 1/2, -z$)	525	2	6	0
A ($-x + 1, y - 1/2, -z + 1/2$)	*B*	368	2	6	0
B	*B* ($x - 1/2, -y + 1/2, -z$)	496	0	2	0
A ($-x + 3/2, -y + 1, z - 1/2$)	*B*	426	1	0	0
A	*A* ($-x + 1, y - 1/2, -z + 1/2$)	366	0	2	0
B	*B* ($-x + 3/2, -y, z - 1/2$)	110	0	0	0

† Symmetry operators are given in parentheses. ‡ The difference in the total accessible surface areas of the isolated and interacting molecules divided by two. § The probability, between 0 and 1, that a crystal-packing interface might represent a real interface.

functional relevance is assigned to the contacts established in the crystal lattice, which is in agreement with the lack of significant contact surfaces in the crystal packing (Table 2). The structures of the two molecules, which were refined independently, are almost identical; after superimposition, the r.m.s.d. in the positions of 106 C$^\alpha$ atoms between the two molecules is 0.39 Å (the maximum-likelihood-based coordinate error of the structure is 0.17 Å). Nevertheless, in one of the molecules there were seven residues (1069–1073 and 1106–1107) which were disordered in the companion molecule.

The Calx-β domain is built up of seven β-strands *A*–*G* (Figs. 1*b* and 1*c*). Strand *A* contains a β-bulge that locally disrupts the hydrogen-bonding pattern; similarly, strand *G* contains a kink at P1095, which makes a *cis*-peptide bond with Q1094. The strands are arranged in two β-sheets, one consisting of strands *G*-*A*-*B*-*E* and the other of strands *D*-*C*-*F*-*G*′-*A*′, which adopt a β-sandwich or Greek-key motif characteristic of the fold in immunoglobulins. The N- and C-termini are located at opposite ends of the longitudinal axis of the structure, which has a cylinder-like shape of about 50 Å in length and ∼24 Å in diameter.

3.2. Comparison with the Ca^{2+}-binding domains of Na$^+$/Ca^{2+} exchanger 1

Superimposition of the Calx-β domain of β4 with the NMR and crystallographic structures of CBD1 and CBD2 of NCX1 reveals a high degree of conservation of the strands that compose the β-sandwich structure (Figs. 2*a* and 2*b*). The r.m.s.d. for a common set of 100 C$^\alpha$ atoms used for pairwise superimposition of the CBDs onto the Calx-β domain of β4 ranges between 0.85 and 1.65 Å (Table 3). The structural similarity is in agreement with the conservation of the sequences; the sequence of the Calx-β domain of β4 is 33% and 27% identical to those of CBD1 and CBD2 of NCX1, respectively. The β4 sequence contains 18 residues that are conserved in CBD1 and CBD2 of NCX1 (Fig. 2*c*), which include 11 residues buried in the core of the β-sandwich (F994, R1014, V1024, T1028, A1033, D1038, F1048, V1059, F1079, L1092 and I1102), three glycines that participate in tight turns of the polypeptide backbone (G1031 and G1093) or in a slight distortion of β-strand *D* (G1044) and three residues that are exposed on the surface of the structure (T1032, E1052 and K1055) and whose side chains engage in intramolecular interactions. Thus, this core of conserved residues contributes to the structural stability of the Calx-β domain. In addition, β4 has another 21 and 14 residues that are conserved in CBD1 and CBD2, respectively. Thus, the Calx-β domain of β4 has nonredundant similarities to both CBD1 and CBD2 of NCX1, suggesting that the β4 domain diverged during evolution before the duplication of the CBDs in the NCX.

The main differences between the Calx-β domain of β4 and those of NCX1 occur at the level of the *BC*, *EF* and *FG* loops. The *BC* loop is stabilized by a hydrogen bond between the carbonyl of G1020 and the side chain of R1014, which makes additional hydrogen bonds with the *DE* loop (Fig. 3*a*). The role of R1014 in β4 is similar to those of R396 and R527 in CBD1 and CBD2 of NCX1, respectively. Nevertheless, the conformation of the *BC* loop is poorly conserved in the three structures; in β4 the structure of the *BC* loop is dictated in part by a hydrogen bond between the N atom of D1018 and the carboxylate group of D990 at the N-terminus of the domain. The *FG* loop of β4 is much shorter than in CBD1 and CBD2 of NCX1 (20 and 39 residues long, respectively) and forms a tight β-hairpin that incorporates a type I′ β-turn (Fig. 3*b*). The presence of G1089, which occupies the γ_L region of the Ramachandran plot ($\varphi = 94^\circ$, $\psi = 1^\circ$), in position $i + 2$ favours the formation of the type I′ turn (Hutchinson & Thornton, 1994). The aromatic ring of F1088 in the *FG* loop is exposed on the surface of the structure and it participates in a cation–π interaction with the side chain of K1021 in the *BC* loop. At the opposite end of the β-sandwich, the *EF* loop is six residues longer in β4 than in the CBDs of NCX1. The *EF* loop does not participate in contacts with other molecules of the crystal lattice and is partially disordered, suggesting that it has a high conformational variability.

3.3. Analysis of the pseudo-Ca^{2+}-binding site of the Calx-β domain of β4

The Ca^{2+}-binding sites of CBD1 and CBD2 of NCX1 are formed by acidic residues that are located in the *AB*, *CD* and *EF* loops and in the C-terminal region downstream of strand *G*. D1038 and D1104 in β4 occupy positions equivalent to D421 and D498 in CBD1, and D552 and E648 in CBD2, which participate in the coordination of Ca^{2+} ions. In contrast, other acidic residues that contribute to the Ca^{2+}-binding site in CBD1 (E385, D447 and E451) and CBD2 (E516, D578 and

Table 3
Structural comparison of the Calx-β domain of β4 with the CBDs of Na^+/Ca^{2+}-exchanger 1.

			C^α r.m.s.d† with integrin β4 Calx-β‡ (Å)	
Domain	Method	PDB code	Molecule *A*	Molecule *B*
CBD1, Ca^{2+}-bound	NMR	2fws	1.65	1.64
CBD1, Ca^{2+}-bound	Crystal	2dpk	0.88	0.85
CBD2, Ca^{2+}-bound	NMR	2fwu	1.33	1.45
CBD2, Ca^{2+}-bound	Crystal	2qvm	0.91	1.05
CBD2, Ca^{2+}-free	Crystal	2qvk	1.01	1.10

† A common set of 100 C^α atoms was used for the comparisons. ‡ Comparison was performed with each of the two molecules present in the asymmetric unit.

E582) of NCX1 are substituted in β4 by either basic or hydrophobic residues: R1003, L1064 and R1074 (Figs. 2*c* and 4). The side chain of R1003 occupies a central position in this region and the guanidinium group occupies positions similar to those of the Ca^{2+} ions in the CBDs of NCX1. In one of the two Calx-β molecules in the asymmetric unit, the guanidinium group of R1003 makes a salt bridge to D1104 and a hydrogen bond to the carbonyl of I1102. In the other molecule R1003 makes a salt bridge to D1038 and a hydrogen bond to the carbonyl of L1062. D1038 makes a salt bridge to R1077, which is very similar to the salt bridge formed between D552 and K585 in the Ca^{2+}-free structure of CBD2 of NCX1. R1074, which in the sequence alignment is equivalent to E451 and E582 of CBD1 and CBD2, respectively (Fig. 2*c*), is oriented with its side chain pointing away from the pseudo-Ca^{2+}-binding region and does not participate in any intramolecular contacts. In summary, the Ca^{2+}-binding sites of the Calx-β domain are not conserved in β4 and they allow charge-compensation interactions that favour stability in the absence of cations.

The initial crystal structure of the Calx-β domain of β4 was obtained in the absence of Ca^{2+}. Therefore, despite the lack of conservation of the Ca^{2+}-binding site, we cannot exclude the possibility that β4 may bind Ca^{2+} *via* a noncanonical mechanism, *e.g.* the *EF* loop contains two acidic residues, E1066 and D1068, which could participate in Ca^{2+} binding. In order to address this issue, we have determined two additional structures of the Calx-β domain at 1.61 and 1.40 Å resolution using crystals grown in the presence of 2 m*M* $CaCl_2$ or grown without calcium but soaked in the presence of 10 m*M* $CaCl_2$, respectively (Table 1). Neither the structure crystallized with Ca^{2+} nor the Ca^{2+}-soaked structure contained ordered cations. No significant differences were observed in the structure of the pseudo-Ca^{2+}-binding region, including the ordered solvent molecules, between the native, the Ca^{2+}-crystallized and the Ca^{2+}-soaked structures (Fig. 5 and Supplementary Fig. 2). The lack of ordered Ca^{2+} in the structure is unlikely to be caused by blockage of the Ca^{2+}-binding site during crystallization. This is supported by the following: (i) the pseudo-Ca^{2+}-binding region of β4 is accessible from the solvent channels of the crystal, (ii) it does not participate in contacts with other molecules of the lattice (Fig. 6) and (iii) the observed conformational freedom of the *EF* loop suggests that it could adapt to bind cations without disrupting the crystal packing. Thus, the absence of ordered Ca^{2+} in the presence of 2 or 10 m*M* $CaCl_2$ suggests that the Calx-β domain of β4 lacks a functional Ca^{2+}-binding site.

In order to compare the crystallographic results with data obtained in solution, we have analyzed the effect of Ca^{2+} on the thermal stability of the Calx-β domain of β4 using a fluorescence-based assay. The thermal denaturation profile of the Calx-β domain in the absence of exogenous cations is characterized by a transition at a T_m of 335 K (Fig. 7). After the initial denaturing process, the samples were cooled and were subjected to a second heating cycle. The T_m value did not change between the first and second melting curves, suggesting that β4 follows a reversible unfolding model which can be considered to be an equilibrium process. No changes were observed in the T_m of β4 in the presence of 10 m*M* $CaCl_2$. Control experiments in the presence of 5 m*M* EGTA showed

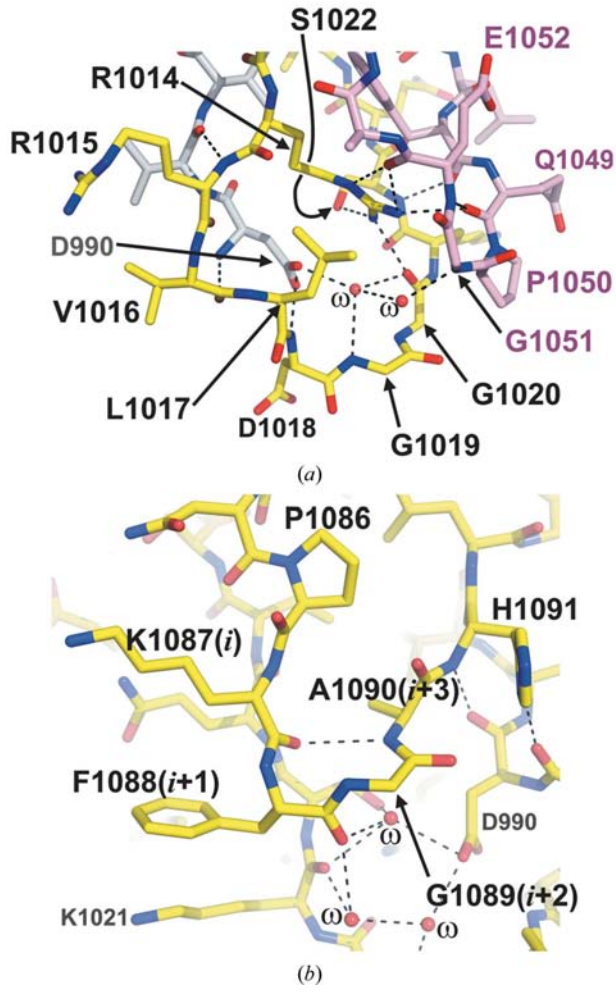

Figure 3
Structure of the *BC*, *DE* and *FG* loops of β4. (*a*) Close-up view of the *BC* (yellow) and *DE* (pink) loops; the side chain of R1014 plays a central role in the stabilization of this region by establishing hydrogen bonds within the *BC* loop and with the backbone of the *DE* loop. D990 in the N-terminus (grey) makes a hydrogen bond to the backbone of the *BC* loop. (*b*) Detailed view of the β-hairpin at the *FG* loop. The relative position of the residues that form the type I′ β-turn (1087–1090) is shown in parentheses. Hydrogen bonds are shown as dashed lines.

the same value of T_m; thus, we can exclude the possibility that the Calx-β domain was stabilized by the presence of residual cations. The lack of effect of calcium on the unfolding of β4 contrasts with the Ca^{2+}-induced thermal stabilization of bona fide Ca^{2+}-binding domains, such as the C2 domains of protein kinase C α, βII and γ (Torrecillas *et al.*, 2004), and the extracellular domains 1 and 2 of E-cadherin (Prasad & Pedigo, 2005).

Finally, binding of Ca^{2+} to the Calx-β domain of β4 was directly analyzed by equilibrium dialysis combined with the determination of Ca^{2+} by ICP-OES. The numbers of Ca^{2+} ions bound per Calx-β domain at free Ca^{2+} concentrations of 155,

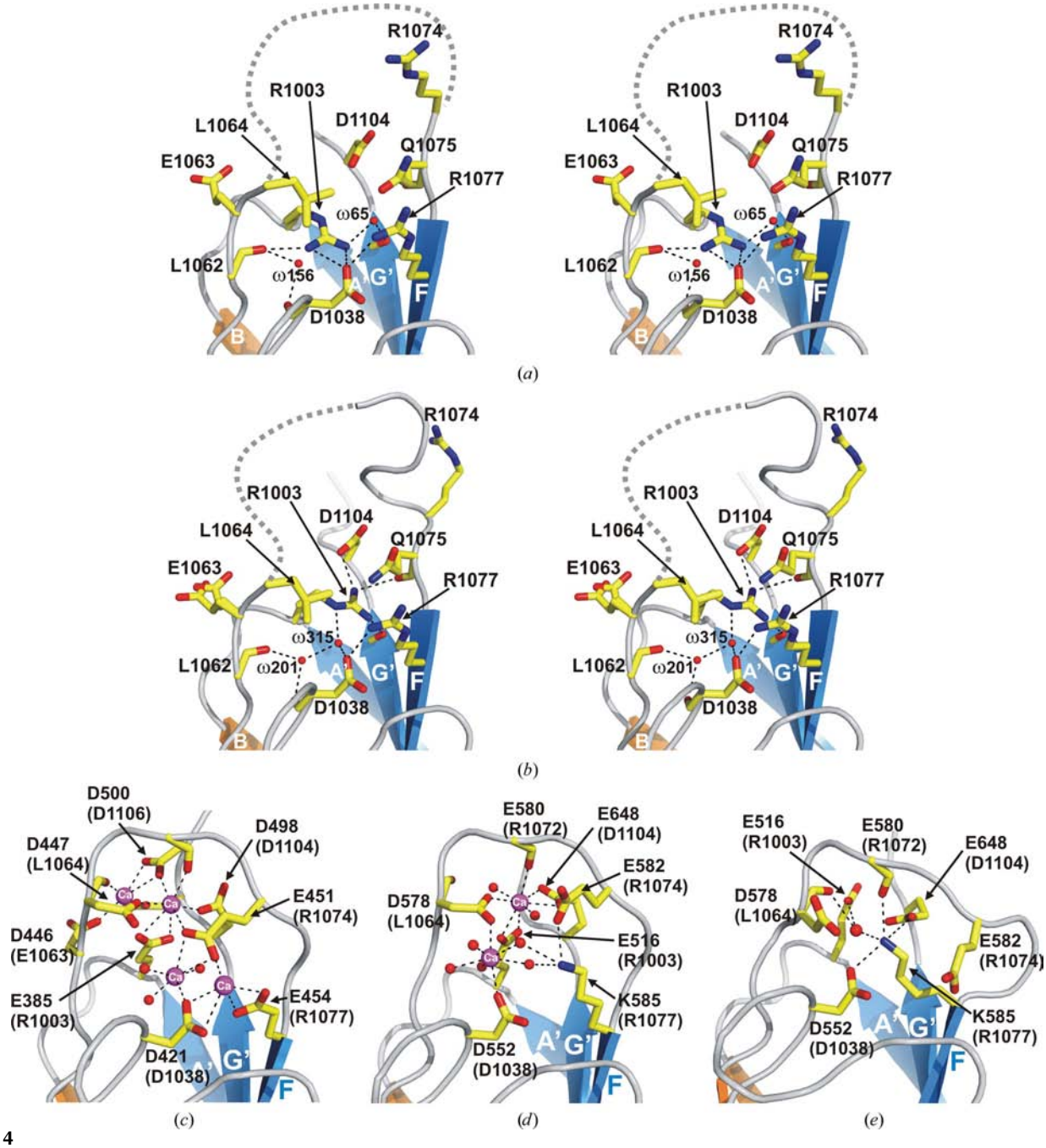

Figure 4
Structure of the region of β4 equivalent to the Ca^{2+}-binding site in Na^+/Ca^{2+}-exchanger 1. (*a*) Stereo representation of the *A′B* and *EF* loops and nearby residues of molecule *A* of β4 present in the asymmetric unit of the crystals. The side chains of residues that occupy positions in the sequence equivalent to residues involved in Ca^{2+} binding in NCX1 are shown as sticks. R1003 was modelled with partial occupancy (refined to a value of 0.91) and was assigned to an alternative conformation to that of the solvent molecule 156, which lies 1.8 Å from the NH1 atom of R1003. The electron density did not allow an unambiguous modelling of other conformers of R1003 (see Fig. 5). (*b*) Stereo representation of the same region of molecule *B* of the asymmetric unit. In this molecule, R1003 forms a salt bridge with D1104. The crystal structures of the Ca^{2+}-binding sites of CBD1 and CBD2 of NCX1 are shown for comparison in (*c*), (*d*) and (*e*). These include (*c*) CBD1 with bound Ca^{2+}, (*d*) CBD2 with bound Ca^{2+} and (*e*) CBD2 in the absence of Ca^{2+}. β4 residues equivalent to those of NCX1 are indicated in parentheses in (*c*), (*d*) and (*e*). Note the similarities of the salt bridge between D1038 and R1077 in β4 and the salt bridge between D552 and K585 in the Ca^{2+}-free structure of CBD2. Polar contacts are shown as dashed lines.

390 and 816 µ*M* were 0.03, 0.02 and 0.13, respectively. In summary, the crystallographic, thermal unfolding and equilibrium dialysis data support the supposition that the Calx-β domain of β4 does not bind Ca^{2+}.

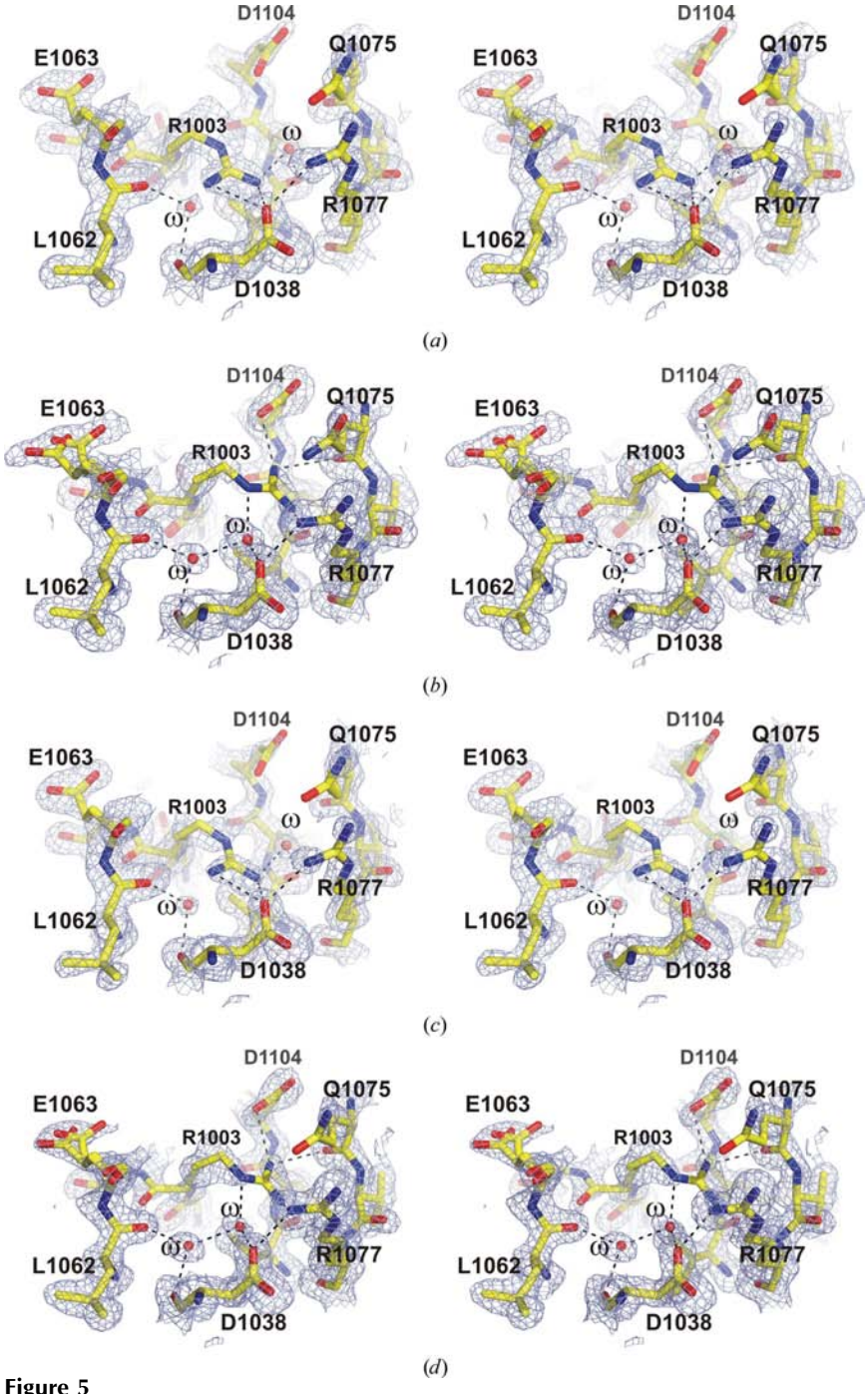

Figure 5
Stereo representations of simulated-annealing OMIT maps of the pseudo-Ca^{2+}-binding sites of the β4 structures. (*a*) Structure of molecule *A* of the asymmetric unit of the native crystal. (*b*) Structure of molecule *B* of the asymmetric unit of the native crystal. (*c*) and (*d*) show the structures of molecule *A* and molecule *B* crystallized in the presence of 2 m*M* Ca^{2+}, respectively. Each map ($2mF_{obs} - DF_{calc}$, contoured at 1σ) was calculated after performing a round of refinement using simulated annealing (initial temperature 5000 K) of models from which the regions shown in the figure were removed. No significant differences were observed in the protein and solvent network between the equivalent molecules of the native and Ca^{2+}-cocrystallized structures.

3.4. Role of R1003 in the stability of the Calx-β domain of β4

In order to asses the role of R1003 on the stability of the Calx-β domain, we have analyzed the thermal stability of two β4 mutants in which R1003 was substituted by Ala or Glu (Fig. 7). The unfolding of the R1003A mutant showed a T_m of 332 K, which is 3 K lower than that of the wild-type protein. CBD1 and CBD2 of NCX1 have a Glu in the position equivalent to R1003. Therefore, we analyzed the effect of substituting R1003 by an acidic residue. The thermal unfolding of the R1003E mutant showed a T_m of 327 K, which is 8 and 5 K lower than the wild type and the R1003A mutant, respectively. The T_m of the R1003E mutant was insensitive to the presence of up to 10 m*M* $CaCl_2$, suggesting that this single substitution is not sufficient to recreate Ca^{2+}-binding site(s) owing to the lack of sequence conservation at the *EF* loop between β4 and the CBDs of NCX1. In summary, the presence of a basic residue in position 1003 contributes to the stability of the Calx-β domain of β4.

4. Discussion

We have determined the crystal structure of the Calx-β domain of β4, which has an overall structural similarity to the CBDs of NCX1, but significant differences at the region equivalent to the Ca^{2+}-binding sites of NCX. The *EF* loop is longer in β4 than in the CBDs and β4 contains basic or non-charged residues in positions equivalent to the acidic residues that participate in the coordination of Ca^{2+} ions in the CBDs of NCX1. Thus, we refer to this region of β4 as a pseudo-Ca^{2+}-binding site. The structures of β4 presented here did not contain Ca^{2+}, even when the crystals were grown in the presence of 2 m*M* $CaCl_2$ or were soaked in mother liquor supplemented with 10 m*M* $CaCl_2$. The pseudo-Ca^{2+}-binding site is characterized by the presence of two basic residues, R1003 and R1077, which engage in intramolecular salt bridges.

The presence of a basic residue, R1003, at the centre of the pseudo-Ca^{2+}-binding site of β4 is unique compared with the CBDs of NCX1, which have Glu residues in the equivalent position (E385 and E516; Supplementary Fig. 3). R1003 appeared in a different conformation in each of the two molecules present in the asymmetric unit. In one molecule R1003 makes a salt bridge with D1038, while it establishes an ionic interaction with D1104 in the other mole-

cule. By combining mutagenesis and thermal unfolding analysis, it was shown that R1003 contributes to the stability of β4. The removal of the side chain of R1003 beyond C^{β} in the R1003A mutant reduces the thermal stability of the Calx-β domain. The destabilizing effect of this substitution is related to the loss of the charge-compensation interactions with D1038 and D1104 and the hydrogen bonds established by the guanidinium group of R1003. Substitution of R1003 by Glu resulted in an additional reduction of the thermal stability, which is likely to be caused by the electrostatic repulsion of the newly introduced carboxylate group with those of D1038 and D1104.

R1077 in β4 has a role similar to that of K585 in CBD2 of NCX1, which in the Ca^{2+}-free state establishes intramolecular salt bridges with D552 and E648. In the absence of Ca^{2+} CBD2 of NCX1 maintains its overall tertiary structure (Hilge *et al.*, 2006), while the Ca^{2+}-binding sites adopt an ordered conformation that facilitates the rapid binding of Ca^{2+} (Besserer *et al.*, 2007). When K585 is substituted by Glu, the mutant CBD2 shows a mild reduction in the apparent affinity for Ca^{2+}, but it undergoes a general structural disorganization upon removal of Ca^{2+} (Besserer *et al.*, 2007; Hilge *et al.*, 2006). In contrast, removing Ca^{2+} from CBD1 of NCX1 induces large structural changes and disorganization of its tertiary structure (Hilge *et al.*, 2006; Johnson *et al.*, 2008; Nicoll *et al.*, 2007; Ottolia *et al.*, 2004). The residue equivalent to R1077 in CBD1 is E454. The substitution E454K results in stabilization of the overall tertiary structure of CBD1 in the absence of Ca^{2+} and a reduction in the apparent affinity for Ca^{2+} (Hilge *et al.*, 2006). In summary, R1077 contributes to the stability of the Calx-β domain of β4 by compensating the negative charge of D1038, in a similar way as K585 stabilizes CBD2 in the absence of Ca^{2+}.

The low sequence conservation and the structural differences of the pseudo-Ca^{2+}-binding site of β4 with respect to that of the CBDs of NCX1 suggest that the Calx-β of β4 is not a Ca^{2+}-binding domain or at least that β4 binds Ca^{2+} in a significantly different way. The structures of β4 derived from crystals grown with 2 m*M* $CaCl_2$ or soaked in 10 m*M* $CaCl_2$ do not reveal bound cations and do not show any noticeable differences from the structure obtained in the absence of Ca^{2+}.

The effect of Ca^{2+} on the thermal stability of the Calx-β domain of β4 was analyzed. In a system in equilibrium in which a ligand binds to the native state but not to the unfolded state, the ligand is expected to stabilize the protein, resulting in an increase of the T_m (Cimmperman *et al.*, 2008). The Ca^{2+}-binding sites of the Calx-β domains of NCX1 include residues from four sequentially distant regions (the *A′B* loop, the *CD* loop, the *EF* loop and the C-terminal region). It is reasonable to assume that in the thermally induced unfolded state Ca^{2+} binding is lost or at least the affinity for Ca^{2+} is severely reduced owing to the structural disorganization of the binding sites. The melting temperature of β4 did not change in the presence of up to 10 m*M* Ca^{2+} with respect to the T_m observed in the absence of divalent cations. Thus, Ca^{2+} did not stabilize the native state of β4, as expected when β4 does not bind Ca^{2+}. Moreover, direct analysis by equilibrium dialysis revealed that a small fraction of Ca^{2+} ions are bound per Calx-β molecule. Collectively, the structural and biophysical data and the results of the sequence-comparison analysis are compatible with the supposition that the Calx-β domain of β4 does not bind Ca^{2+}.

What role does the Calx-β domain play in the context of the cytoplasmic domain of the β4 subunit? The Calx-β and the four FnIII repeats are the only globular domains identified in the cytoplasmic region of β4 and they account for about half of its sequence. These domains belong to the immunoglobulin superfamily, their size is similar and they are characterized by having their N- and C-termini at opposite ends along the

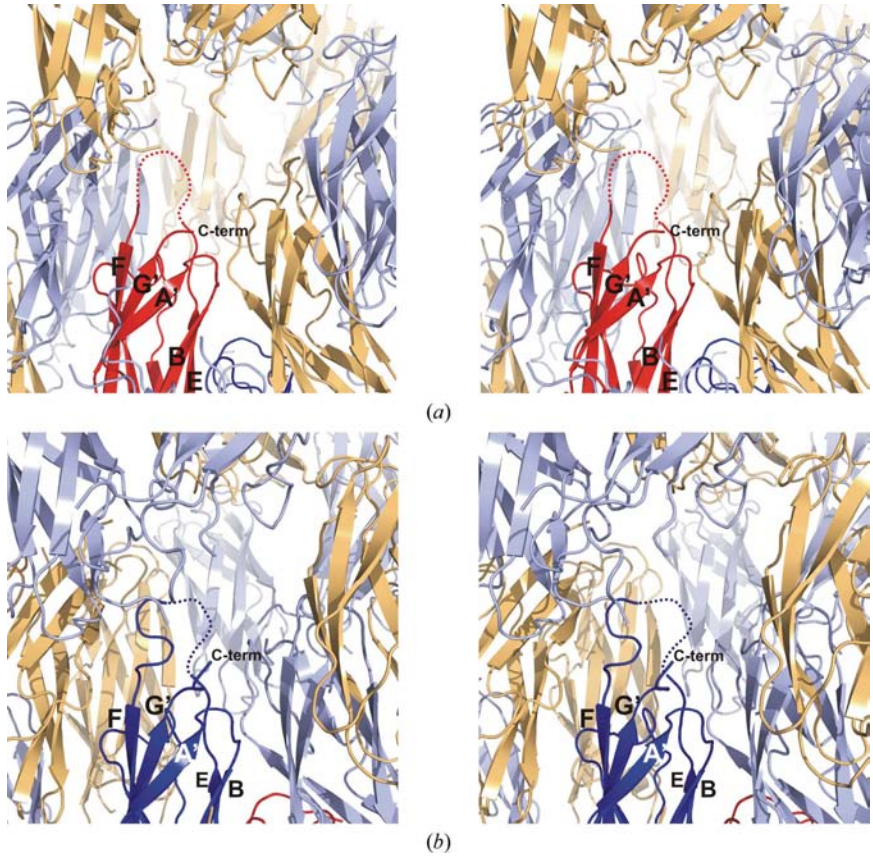

Figure 6
Crystal-packing environment of the pseudo-Ca^{2+}-binding site of the Calx-β domain of β4. (*a*) Stereo ribbon representation of molecule *A* of the asymmetric unit (red) and neighbouring molecules in the crystal lattice. (*b*) Equivalent representation for molecule *B* (dark blue) of the asymmetric unit. In both panels, symmetry-related copies of the *A* and *B* molecules are coloured orange and light blue, respectively. A region of the *EF* loops which is partially disordered in both copies is shown as a dashed line.

longitudinal axis of the structure, suggesting that the cytoplasmic region of β4 has a beads-on-a-string organization. The Calx-β domain is linked to the first FnIII domain by an ~20-residue-long sequence that is likely to act as a flexible hinge. The length of this linker is similar to that of the linker that connects the third and fourth FnIII domains. In contrast, the first and second FnIII domains are connected by a zero-length linker and adopt an apparently rigid rod-like structure both in the crystals (de Pereda *et al.*, 1999) and in solution (Chacon *et al.*, 2000).

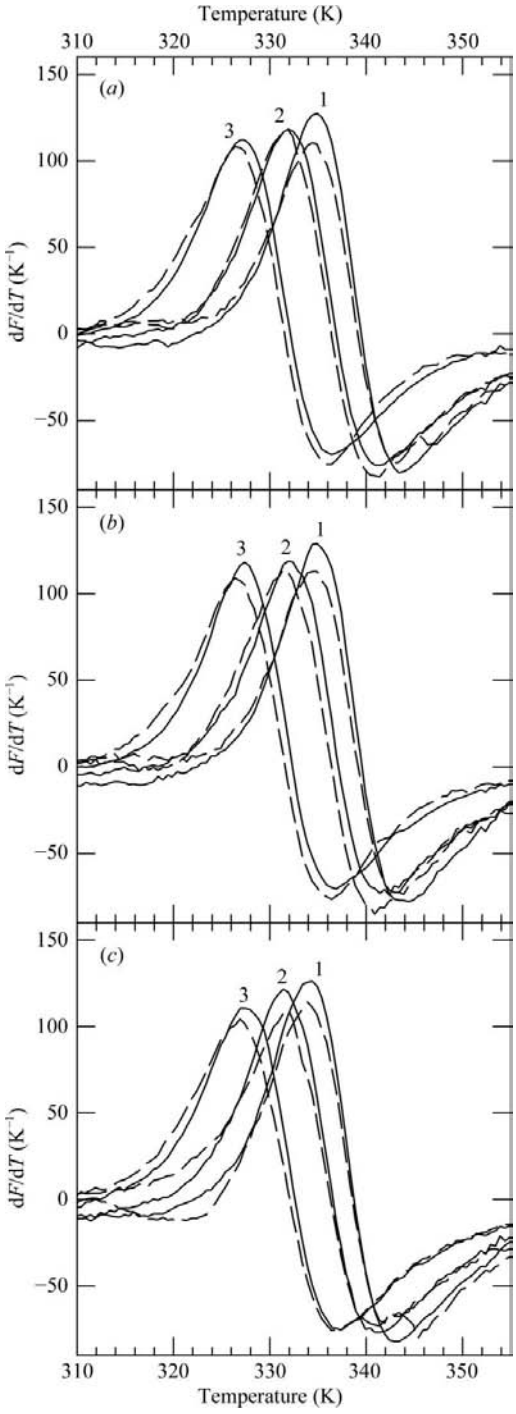

Figure 7
Thermal unfolding of the Calx-β domain of β4. (*a*) Representative thermofluor unfolding curves of the wild type (1) and the R1003A (2) and R1003E mutants (3) in 50 m*M* HEPES pH 7.5, 150 m*M* NaCl. Solid lines correspond to the first heating pass, while the companion curves in dashed lines correspond to a subsequent temperature scan performed after cooling the samples. (*b*) Unfolding in 50 m*M* HEPES pH 7.5, 150 m*M* NaCl, 5 m*M* EGTA and (*c*) in 50 m*M* HEPES pH 7.5, 150 m*M* NaCl, 10 m*M* $CaCl_2$. The T_m of the unfolding transition did not change, within experimental error, in the presence of 10 m*M* $CaCl_2$ or in the presence of 5 m*M* EGTA.

To date, no specific function has been assigned to the Calx-β domain of β4. The cytoplasmic region of β4 is cleaved in a Ca^{2+}-dependent manner *in vivo* and calpain digests β4 *in vitro* (Giancotti *et al.*, 1992), which has led to the proposition that the Calx-β domain could be involved in the regulation of the proteolytic processing of the β4 subunit (May & Ponting, 1999). Nonetheless, calpain digests β4 at two sites that are probably located in the second FnIII domain and the connecting segment (Giancotti *et al.*, 1992), but not in the Calx-β domain. In addition, our data suggest that the Calx-β domain does not bind Ca^{2+}; hence, it would not act as a Ca^{2+}-sensor. Thus, it is unlikely that the Calx-β domain is involved in the regulation of the Ca^{2+}-induced processing of β4.

The cytoplasmic moiety of β4 acts as a protein–protein interaction platform both in cell adhesion and signalling events. Of the five globular domains of the β4 cytoplasmic region, the four FnIII domains mediate association with other proteins, including hemidesmosomal components (Geerts *et al.*, 1999; Koster *et al.*, 2003, 2004) and signalling molecules (Bertotti *et al.*, 2006; Dans *et al.*, 2001). Therefore, it is possible that the Calx-β domain of β4, which is structurally related to the FnIII fold, is also involved in protein–protein interactions. The Src-family kinase Fyn associates with the $\alpha6\beta4$ integrin in response to EGF stimulation, leading to phosphorylation of the β4 subunit. The association with Fyn requires the transmembrane-proximal region of β4, residues 854–1183, which contains the Calx-β domain (residues 989–1107) (Mariotti *et al.*, 2001). Thus, the Calx-β domain might participate in protein–protein interactions during $\alpha6\beta4$ signalling. Finally, the Calx-β domain of β4 might play a role in maintaining the structural organization of the β4 cytodomain contributing to the correct presentation of other protein-interaction modules, such as the FnIII domains.

The potential functional sites (*e.g.* intermolecular or intramolecular protein-interaction sites) in the Calx-β domain of β4 are likely to correspond to areas that are not conserved in other domains. 45% of the sequence of the β4 domain is identical to the sequence of CBD1 or CBD2 of NCX1 (Fig. 2*c*). The largest regions of β4 that are not conserved in either of the NCX1 domains are the *A′B* loop, the first half of strand *B*, the *EF* loop and the *FG* loop. The *A′B* and *EF* loops are located adjacent to each other at one of the ends of the β-sandwich. The equivalent region in the CBDs of NCX1 corresponds to the Ca^{2+}-binding sites. It is reasonable that this tip of the Calx-β domain has evolved to fulfil different functions in NCXs and β4. The extension of the *EF* loop of β4 (^{1062}LELQEVDSLLRGRQ^{1075}), which is longer than that of other Calx-β domains and bears no sequence similarity to them (Supplementary Fig. 3), is of interest. In the fold of

immunoglobulins, function-specific sequences are frequently present in loops. For example, the tenth FnIII domain of fibronectin contains an RGD integrin-binding motif in the flexible *FG* loop (Dickinson *et al.*, 1994). Thus, we propose that the apical surface formed by the *A′B* and *EF* loops of the Calx-β domain of β4 may constitute a functional site.

In summary, the three-dimensional structure of the Calx-β domain and the identification of a potential functional surface should be helpful in designing novel experiments aimed at unveiling the role of this domain in the function of the $\alpha6\beta4$ integrin both in normal epithelium and in tumour progression.

We thank Anastassis Perrakis, Jaime Pascual, Tina Bakolitsa and Margarita Menéndez for critical reading of the manuscript and suggestions. We thank Antonio Romero for generous access to the X-ray equipment at the Centro de Investigaciones Biológicas (CSIC, Madrid). This work was supported by the Spanish Ministry of Science and Innovation and the European Regional Development Fund (grant BFU2006-01929/BMC to JMdP). NAG is the recipient of a JAE predoctoral research training grant from the Consejo Superior de Investigaciones Cientificas. AIP was the recipient of a fellowship for undergraduate students from the Spanish Ministry of Education and Science.

References

Afonine, P. V., Grosse-Kunstleve, R. W. & Adams, P. D. (2005). *CCP4 Newsl.* **42**, contribution 8.
Arnaout, M. A., Goodman, S. L. & Xiong, J. P. (2007). *Curr. Opin. Cell Biol.* **19**, 495–507.
Bertotti, A., Comoglio, P. M. & Trusolino, L. (2006). *J. Cell Biol.* **175**, 993–1003.
Besserer, G. M., Ottolia, M., Nicoll, D. A., Chaptal, V., Cascio, D., Philipson, K. D. & Abramson, J. (2007). *Proc. Natl Acad. Sci. USA*, **104**, 18467–18472.
Canutescu, A. A., Shelenkov, A. A. & Dunbrack, R. L. Jr (2003). *Protein Sci.* **12**, 2001–2014.
Chacon, P., Diaz, J. F., Moran, F. & Andreu, J. M. (2000). *J. Mol. Biol.* **299**, 1289–1302.
Cimmperman, P., Baranauskiene, L., Jachimoviciute, S., Jachno, J., Torresan, J., Michailoviene, V., Matuliene, J., Sereikaite, J., Bumelis, V. & Matulis, D. (2008). *Biophys. J.* **95**, 3222–3231.
Dans, M., Gagnoux-Palacios, L., Blaikie, P., Klein, S., Mariotti, A. & Giancotti, F. G. (2001). *J. Biol. Chem.* **276**, 1494–1502.
Davis, I. W., Leaver-Fay, A., Chen, V. B., Block, J. N., Kapral, G. J., Wang, X., Murray, L. W., Arendall, W. B. III, Snoeyink, J., Richardson, J. S. & Richardson, D. C. (2007). *Nucleic Acids Res.* **35**, W375–W383.
DeLano, W. L. (2002). *The PyMOL Molecular Graphics System.* DeLano Scientific, San Carlos, California, USA.
Dickinson, C. D., Veerapandian, B., Dai, X. P., Hamlin, R. C., Xuong, N. H., Ruoslahti, E. & Ely, K. R. (1994). *J. Mol. Biol.* **236**, 1079–1092.
Diederichs, K. & Karplus, P. A. (1997). *Nature Struct. Biol.* **4**, 269–275.
Emsley, P. & Cowtan, K. (2004). *Acta Cryst.* D**60**, 2126–2132.
Fernandez-Busquets, X., Kammerer, R. A. & Burger, M. M. (1996). *J. Biol. Chem.* **271**, 23558–23565.
Flier, A. van der & Sonnenberg, A. (2001). *Cell Tissue Res.* **305**, 285–298.
Geerts, D., Fontao, L., Nievers, M. G., Schaapveld, R. Q., Purkis, P. E., Wheeler, G. N., Lane, E. B., Leigh, I. M. & Sonnenberg, A. (1999). *J. Cell Biol.* **147**, 417–434.
Giancotti, F. G. (2007). *Trends Pharmacol. Sci.* **28**, 506–511.
Giancotti, F. G., Stepp, M. A., Suzuki, S., Engvall, E. & Ruoslahti, E. (1992). *J. Cell Biol.* **118**, 951–959.
Hayase, M., Maekawa, A., Yubisui, T. & Minami, Y. (2008). *Int. J. Biochem. Cell Biol.* **40**, 2141–2150.
Hilge, M., Aelen, J. & Vuister, G. W. (2006). *Mol. Cell*, **22**, 15–25.
Hodor, P. G., Illies, M. R., Broadley, S. & Ettensohn, C. A. (2000). *Dev. Biol.* **222**, 181–194.
Holm, L. & Park, J. (2000). *Bioinformatics*, **16**, 566–567.
Hutchinson, E. G. & Thornton, J. M. (1994). *Protein Sci.* **3**, 2207–2216.
Hynes, R. O. (2002). *Cell*, **110**, 673–687.
Jaroszewski, L., Rychlewski, L., Li, Z., Li, W. & Godzik, A. (2005). *Nucleic Acids Res.* **33**, W284–W288.
Johnson, E., Bruschweiler-Li, L., Showalter, S. A., Vuister, G. W., Zhang, F. & Bruschweiler, R. (2008). *J. Mol. Biol.* **377**, 945–955.
Kabsch, W. (1976). *Acta Cryst.* A**32**, 922–923.
Kabsch, W. (1993). *J. Appl. Cryst.* **26**, 795–800.
Kiyozumi, D., Sugimoto, N., Nakano, I. & Sekiguchi, K. (2007). *Matrix Biol.* **26**, 456–462.
Koster, J., Geerts, D., Favre, B., Borradori, L. & Sonnenberg, A. (2003). *J. Cell Sci.* **116**, 387–399.
Koster, J., van Wilpe, S., Kuikman, I., Litjens, S. H. & Sonnenberg, A. (2004). *Mol. Biol. Cell*, **15**, 1211–1223.
Krissinel, E. & Henrick, K. (2007). *J. Mol. Biol.* **372**, 774–797.
Lipscomb, E. A. & Mercurio, A. M. (2005). *Cancer Metastasis Rev.* **24**, 413–423.
Litjens, S. H., de Pereda, J. M. & Sonnenberg, A. (2006). *Trends Cell Biol.* **16**, 376–383.
Lovell, S. C., Davis, I. W., Arendall, W. B. III, de Bakker, P. I., Word, J. M., Prisant, M. G., Richardson, J. S. & Richardson, D. C. (2003). *Proteins*, **50**, 437–450.
Lytton, J. (2007). *Biochem. J.* **406**, 365–382.
Mariotti, A., Kedeshian, P. A., Dans, M., Curatola, A. M., Gagnoux-Palacios, L. & Giancotti, F. G. (2001). *J. Cell Biol.* **155**, 447–458.
May, A. P. & Ponting, C. P. (1999). *Trends Biochem. Sci.* **24**, 12–13.
McCoy, A. J., Grosse-Kunstleve, R. W., Storoni, L. C. & Read, R. J. (2005). *Acta Cryst.* D**61**, 458–464.
Nicoll, D. A., Ren, X., Ottolia, M., Phillips, M., Paredes, A. R., Abramson, J. & Philipson, K. D. (2007). *Ann. NY Acad. Sci.* **1099**, 1–6.
Nicoll, D. A., Sawaya, M. R., Kwon, S., Cascio, D., Philipson, K. D. & Abramson, J. (2006). *J. Biol. Chem.* **281**, 21577–21581.
Niessen, C. M., Hulsman, E. H., Oomen, L. C., Kuikman, I. & Sonnenberg, A. (1997). *J. Cell Sci.* **110**, 1705–1716.
Nievers, M. G., Schaapveld, R. Q. & Sonnenberg, A. (1999). *Matrix Biol.* **18**, 5–17.
Nikkila, H., McMillan, D. R., Nunez, B. S., Pascoe, L., Curnow, K. M. & White, P. C. (2000). *Mol. Endocrinol.* **14**, 1351–1364.
Ottolia, M., Philipson, K. D. & John, S. (2004). *Biophys. J.* **87**, 899–906.
Pace, C. N., Vajdos, F., Fee, L., Grimsley, G. & Gray, T. (1995). *Protein Sci.* **4**, 2411–2423.
Painter, J. & Merritt, E. A. (2006). *Acta Cryst.* D**62**, 439–450.
Pantoliano, M. W., Petrella, E. C., Kwasnoski, J. D., Lobanov, V. S., Myslik, J., Graf, E., Carver, T., Asel, E., Springer, B. A., Lane, P. & Salemme, F. R. (2001). *J. Biomol. Screen.* **6**, 429–440.
Pereda, J. M. de, Lillo, M. P. & Sonnenberg, A. (2009). *EMBO J.* **28**, 1180–1190.
Pereda, J. M. de, Wiche, G. & Liddington, R. C. (1999). *EMBO J.* **18**, 4087–4095.
Prasad, A. & Pedigo, S. (2005). *Biochemistry*, **44**, 13692–13701.

Sambrook, J., Fritsch, E. F. & Maniatis, T. (1989). *Molecular Cloning: A Laboratory Manual*, 2nd ed. New York: Cold Spring Harbor Laboratory Press.
Schwarz, E. M. & Benzer, S. (1997). *Proc. Natl Acad. Sci. USA*, **94**, 10249–10254.
Theobald, D. L. & Wuttke, D. S. (2006). *Bioinformatics*, **22**, 2171–2172.
Torrecillas, A., Laynez, J., Menendez, M., Corbalan-Garcia, S. & Gomez-Fernandez, J. C. (2004). *Biochemistry*, **43**, 11727–11739.
Wegener, K. L. & Campbell, I. D. (2008). *Mol. Membr. Biol.* **25**, 376–387.
Wilhelmsen, K., Litjens, S. H. & Sonnenberg, A. (2006). *Mol. Cell. Biol.* **26**, 2877–2886.